AIAA SCITECH 2025 Forum, 6-10 January 2025 Orlando, FL. Paper number AIAA 2025-0479
DOI:10.2514/6.2025-0479

Impact of Whale Tubercles on the Aerodynamics Characteristics of F1 Front Wing

Fidel Toprakoglu*, Ismet Ozyumruoglu†, Zeeshan A. Rana‡, Davide Di Pasquale§, Simon Prince¶
School of Aerospace, Transport and Manufacturing, Cranfield University, UK, MK43 0AL
Department of Mechanical Engineering, Prince Mohammad Bin Fahd University, Al-Khobar, KSA

This research aimed to investigate the impact of varying tubercles frequency and amplitude on the leading edge of a double-element Formula One (F1) front wing at two different ride heights in the pre-stall regime. A bio-inspired tubercle distribution was implemented, varying in amplitude and frequency across the span. Computational simulations were performed at 30m/s using the $\kappa - \omega$ SST model. The results showed that implementing bio-inspired tubercles on front wings did not improve aerodynamic efficiency at any ride height. The clean leading-edge model consistently achieved the highest lift-to-drag ratio at both ride heights. Configurations with various tubercle amplitude presented different results: for low-amplitude tubercles, the downforce increased compared to the baseline at the cost of increased drag. Models with higher amplitude tubercles led to significant downforce reduction due to flow separation, further diminishing aerodynamic performance. Variations in tubercle frequency had minimal impact on aerodynamic performances. Among the tubercle configurations tested, the model with the lowest amplitude and the fewest tubercles achieved the highest aerodynamic efficiency.

I. Nomenclature

A	=	amplitude of tubercles
C_D	=	drag coefficient
C_L	=	lift coefficient
C_p	=	pressure coefficient
CFD	=	Computational Fluid Dynamics
c	=	chord [mm]
f_x	=	frequency of tubercles (x number of tubercles)
F1	=	Formula 1
G_R	=	growth rate
h	=	height [mm]
h/c	=	ride height
H	=	domain height
L_c	=	domain chordwise length
L_d	=	domain downstream length
L_u	=	domain upstream length
NASA	=	National Aeronautics and Space Administration
Re	=	Reynolds number
SST	=	Shear Stress Transport
x/c	=	normalised chordwise direction

*Researcher, Centre for Aeronautics, Cranfield University, UK.
†Researcher, Centre for Aeronautics, Cranfield University, UK.
‡Associate Professor, Prince Mohammad Bin Fahd University, Al-Khobar, KSA; Member AIAA.
§Lecturer, Centre for Aeronautics, Cranfield,UK, Senior Member AIAA
¶Professor, Center for Aeronautics, Cranfield University, UK, Senior Member AIAA.

II. Introduction

In motorsport, and especially in Formula One (F1), a gain of a tenth of a second can be decisive for winning. In this context, new concepts and innovations are consistently developed to push the limits of speed and precision further and establish a competitive advantage on the racetrack. Performance enhancement can be achieved through improvements to the engine, the chassis or the aerodynamics of the car which is the most significant factor to enhance overall performance and yield substantial gains in performance. The front wing in F1 cars is crucial as it generates 30% of the total downforce to ensure grip, directing the airflow around the car to reduce drag and thus increase speed. Its significance cannot be overstated, as even slight modifications to its setup can have substantial effects on the vehicle's performance and competitiveness on the racetrack.

To optimize the flow behaviour and enhance performance, flow control techniques can be used. They can be passive (changes in shape or surface characteristics) or active (use of external energised mechanisms). These techniques aim to add energy and enhance mixing within the boundary layer to delay transition or separation and improve aerodynamic performance. In this study, a passive flow control, inspired by the humpback whale's flippers called tubercles was investigated. The implementation of leading-edge tubercles on wings has seen more and more interest nowadays for its aerodynamic performance enhancement in the post-stall regime. Tubercles are protuberances located on the leading edge of humpback whale's flippers allowing them to realise acrobatic underwater manoeuvres and provide extra mobility.

Fig. 1 Humpback whale's flipper. Photography of George Karbus [1]

Fish *et al.* [2] were the first to study the aerodynamic effects of implementing tubercles. Since then, aerodynamic performance enhancement through the implementation of tubercles has been extensively investigated. For instance, Watts and Fish [3] developed a panel method to run simulations to observe the effects of tubercles on wing performance. They showed that for large Reynolds number, at 10 degrees, an increase of 4.8% in lift and a decrease of 10.9% in drag led to an increase of 17.6% in lift-to-drag ratio. Nonetheless, the exact mechanism in which the tubercles alter the flow behavior remains unknown. Miklosovic *et al.* [4] proposed that tubercles act like vortex generators: by generating streamwise vortices they enhance momentum exchange within the boundary layer to keep the flow attached and thus avoid separation which maintains lift at high angles of attack and consequently delays stall. Thereby, pressure drag is strongly reduced in the post-stall regime. According to Van Nierop *et al.* [5], in the downwash region, the effective angle of attack is reduced, which delays the separation behind the peaks, whereas it increases the effective angle of attack in the upwash region, which favours separation. Therefore, since the effect of vortices in the downwash is higher [6], this results in a more gradual and less abrupt stall. Similarly, Custodio [7] considered tubercles to act like delta wings. The vortices generated help to produce high lift even at high angles of attack and the downwash keeps the flow behind the peaks attached which delays stall. Watts and Fish [3] saw tubercles as wing fences. The generated vortices are better distributed along the span which reduces spanwise flow. Separation is confined and only happens at the tip as numerically shown by Pedro *et al.* [8] ($Re = 5\times10^5$). In addition to that, the strength of the tip vortices is reduced and therefore induced drag as well [8–10].

Moreover, for flow around $Re \approx 5 \times 10^5$ tubercles improve the post-stall regime by delaying stall and reducing

its severity, lift is enhanced and drag is reduced [4, 5, 8]. Although a consensus on the fact that tubercles delay stall and are efficient in the post-stall regime seems to be found, discrepancies exist among researchers concerning their effects in the pre-stall regime ([3, 9–11] for respectively large Reynold numbers, $Re = 2 \times 10^5$, $Re = 5 \times 10^5$ to 1×10^6 and $Re = 1.8 \times 10^5$). All these discrepancies show another key factor: the impact of the Reynolds number. Much of the research has been conducted at different Reynolds numbers and shows that the impact of the tubercles is Reynolds-dependant as shown by Hansen [12].

The main geometric parameters of tubercles that affect the effectiveness are their amplitude and wavelength (or frequency). Van Nierop *et al.* [5] observed that increasing the amplitude would increase the aerodynamic performance for $Re > 5 \times 10^5$. They also observed that stall delay was insensitive to the wavelength of tubercles. Similarly, Johari *et al.* [11] concluded that the amplitude has the main impact on performance whereas the frequency of the tubercles plays a minor role. However, they found that the optimal performance was achieved by reducing the tubercles' amplitude. For low Reynolds numbers, Hansen *et al.* [13] also observed that reducing tubercle amplitude provides better performance. Moreover, they compared the effect of varying tubercle frequency. It was observed that as the spacing between tubercles decreased, performance was improved. However, they found a certain point beyond which further reduction of wavelength would deteriorate performance, suggesting an optimum configuration for each case. In fact, Arrondeau [14] also suggests that tubercles are case-dependent and that an optimal configuration for tubercle implementation exists for any geometry. Finally, for Reynolds numbers from 3.5×10^4 to Srinivas *et al.* [15] demonstrated that a bio-mimicked (non-constant amplitude and frequency of tubercles along the span) marine rudder has a better performance than a uniform tubercle distribution in the transitory-turbulent regime ($Re \approx 10^5$): higher lift and a less severe stall in the post-stall regime. In the pre-stall regime, lift decreases compared to a smooth wing but lift is enhanced compared to a wing with tubercles with constant amplitude and frequency. Therefore, the performance for an optimised wing with tubercles is as great as a smooth clean wing [12, 15].

The "Ground effect" is used by motorsport engineers to improve the generated downforce. Indeed, this phenomenon can be explained by Venturi's effect: the proximity of the front wing to the ground creates a reduction in the cross-sectional area in which the air is flowing which accelerates the air and consequently decreases the static pressure under the front wing and generates a downforce. Zerihan's work on his PhD thesis is a pioneer in this subject [16]. He conducted experiments and CFD simulations and showed that the generated downforce of a single-element wing in ground effect asymptotically increases as the ride height decreases until it reaches a maximum value of the downforce. Below that optimum ride height, the generated downforce significantly drops. Therefore, a higher loading, suction is experienced by the wing. This tendency was also experimentally and numerically confirmed throughout the literature [17–22]. The ground effect enhances downforce by generating higher suction. Zerihan observed this enhancement in downforce on a double-element wing in ground effect and attributed it to the suction generated by the main plane vortices [16]. Mahon associated the drop in downforce with the breakdown of these vortices and that the use of endplate feet helps to maintain these vortices and thus the downforce [18]. Moreover, the optimum range of ride heights is narrow and out of this range, the wing experiences a drop in performance and stability [17].

The optimisation of an F1 front wing consist of downforce enhancement, drag reduction and achieving an optimum value of the lift-to-drag ratio to improve cornering and straight-line speeds, reduce fuel consumption, and improve stall margins. Few researches have been conducted on implementing tubercles on an F1 front wing in ground effect to enhance its performance and optimize the tubercles' configuration.

B. Arrondeau and Z. A. Rana [14] conducted a parametric optimisation on a double-element front wing to find the optimum values for tubercles' amplitude and frequency. They showed that, in stall conditions, implementing tubercles at a ride height of height-to-chord ratio $(h/c) = 0.211$ enhanced the aerodynamic performance in the post-stall regime (Re: downforce is increased by 22.6%, lift-to-drag ratio by 9.4%) and stall on the main plane is delayed due to the generation of streamwise vortices that enhance boundary layer mixing. However, this increase in performance occurs to the detriment of an increase in drag. Moreover, even though higher amplitude seems to be better as it reduces the size of the recirculation zone, the overall aerodynamic performance (*i.e.* lift-to-drag ratio) is reduced. S. Angad [23] continued the study on the effect of tubercle frequency. He observed an optimal tubercle distribution of 20 protrusions on the leading edge. Nonetheless, he found that for a ride height of $h/c = 0.172$, the clean configuration offers better aerodynamic performance than the configurations with tubercles as it generates more downforce.

This research aims to investigate the effects of tubercles on a double element F1 front wing in ground effect similar to the one used by Zerihan [16]. Two ride heights were investigated: $h/c = 0.134$ and $h/c = 0.224$. Numerical simulations were performed to assess the aerodynamic performance of several configurations with constant and varying amplitude and frequency of tubercles. The next section focuses on the explanation of the investigated geometries and the computational framework along with the presentation of the meshes generated and the flow conditions. Finally, the results of the numerical simulations and the adjoint optimization were analyzed in line with the physics of the flow to gain a better understanding and identify the best-performing configuration regarding Formula 1 applications.

III. Computational Framework

A. Baseline geometry

The baseline geometry of this aerodynamic study was a double-element Formula 1 front wing with a rectangular endplate. It was the same geometry used by Zerihan in his thesis [16]. The main element wing profile was a modified NASA GA(W) profile, type LS(1)-0413 MOD. The chord of the main element was 223 mm and the flap had a chord of 165 mm resulting in a chord of 380 mm for the two airfoils. This dimension was used as the reference length for the non-dimensional calculations. The effective incidence of the two elements was 14.1°. The overlap and the gap between the main element and the flap were 0.024c and 0.032c. The endplates were rectangular and measure 400 mm × 170 mm × 4 mm. The endplate was used for the validation case but was removed later when compared with the tubercle configurations. The total span of the front wing is 1100 mm. The geometry is displayed in figure 2. To reduce the computational cost, the simulations were performed using only half of the geometry corresponding to a span of 550mm, using a symmetry boundary condition. To better observe the impact of implementing tubercles, the study was realised at two different ride heights: $h/c = 0.134$ and $h/c = 0.224$. These ground heights resulted in a ground clearance of $50.92mm$ and $85.12mm$ respectively.

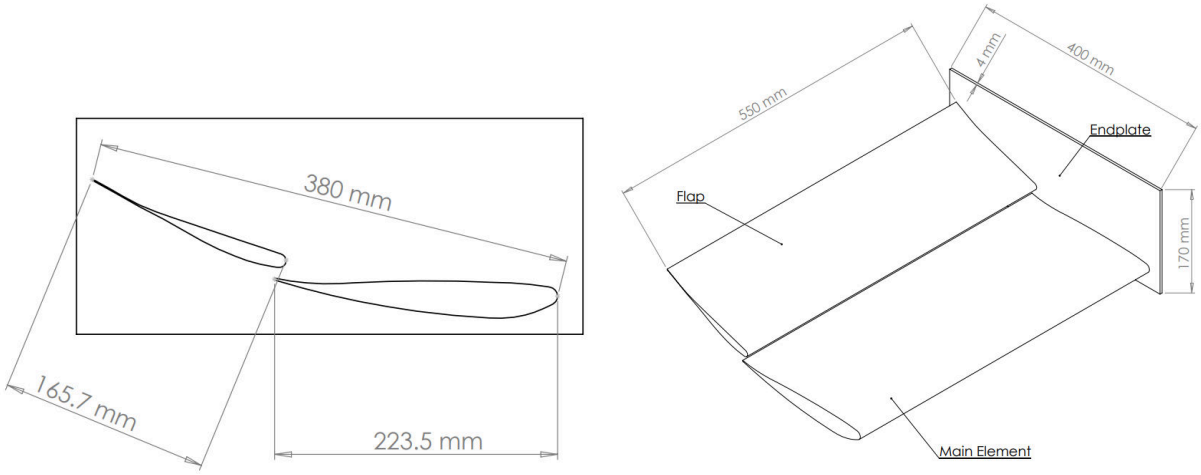

Fig. 2 Double element front wing used in numerical simulations

B. Tubercle configurations

Eight configurations including the clean leading-edge model were created and tested. To replicate a bio-mimicked tubercle implementation, it was decided to vary both tubercle frequency and amplitude along the spanwise direction of the F1 front wings. All the front wing models have a constant thickness-to-chord ratio, including the tubercle configurations. The configurations were tested at both ride heights.

A nomenclature describing the tubercles frequencies and amplitude at the root and tip half was proposed: $MEF\_f_X\_2AX\_f_Y\_2AY$ where MEF stood for tubercles on both the main element and the flap, F_X_2AX was the frequency and amplitude at the root half and F_Y_2AY the frequency at the tip half. For instance, the configuration $MEF\_f_3\_2A004\_f_6\_2A002$ had 9 tubercles on both the main element and the flap. On the root half of the span, there

were 3 tubercles. The amplitude from the peaks to the troughs was $2A = 0.04c$ with respect to the baseline. The tip half contained 6 tubercles with an amplitude of $2A = 0.02c$.

Figure 3 presents a schematic representation of the definition of the configurations with tubercles. Configurations displayed in Figure 4 aimed to study the impact of tubercle frequency. On the other hand, configurations illustrated in Figure 5 were used to study amplitude's impact on aerodynamic behaviour.

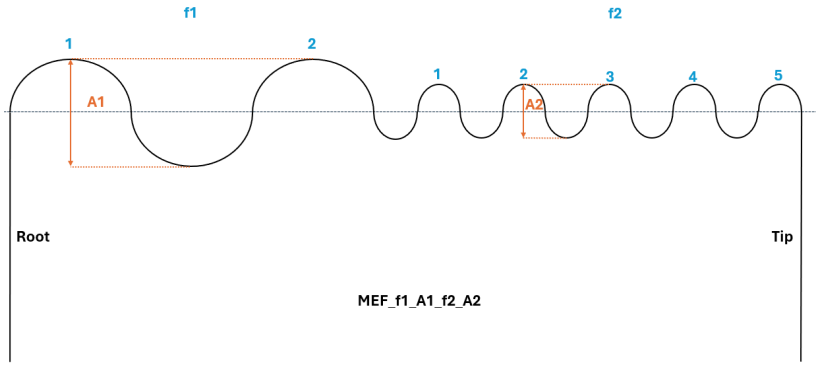

Fig. 3 Tubercles configuration schematic definition.

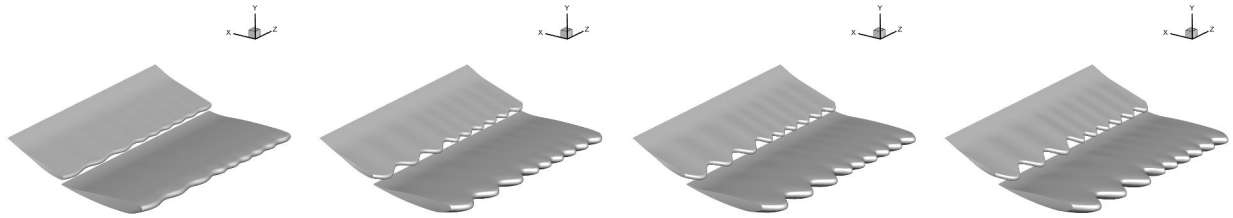

(a) $MEF\_f_3\_2A004\_f_6\_2A002$ (b) $MEF\_f_3\_2A006\_f_6\_2A003$ (c) $MEF\_f_3\_2A008\_f_6\_2A004$ (d) $MEF\_f_3\_2A010\_f_6\_2A005$

Fig. 4 First set of tubercles configurations (Amplitude analysis)

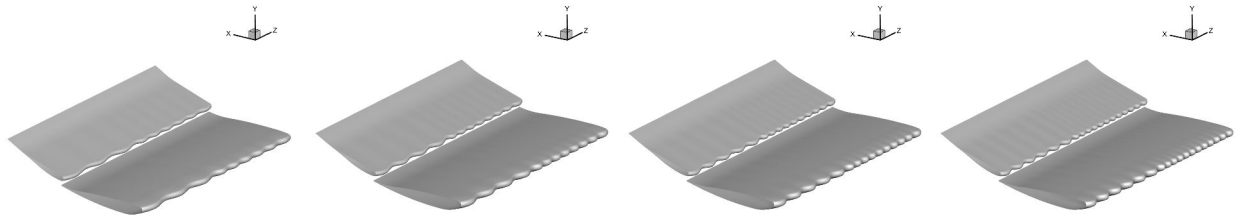

(a) $MEF\_f_3\_2A004\_f_6\_2A002$ (b) $MEF\_f_4\_2A004\_f_8\_2A002$ (c) $MEF\_f_5\_2A004\_f_{10}\_2A002$ (d) $MEF\_f_6\_2A004\_f_{12}\_2A002$

Fig. 5 Second set of tubercles configurations (Frequency analysis).

C. Computational domain

A H-type mesh was chosen to perform the numerical simulations. The rectangular domain can be characterized by four dimensions: H for the box height, L_c for the crosswise length, L_d for the downstream length and L_u for the upstream. Table 1 recapitulates the dimensions used in the literature. Based on that, a numerical domain was established

whose dimensions was 8c in width and height, 9c upstream and 15c downstream the geometry. In addition, two refinement boxes were used: a very fine mesh region around the front wing and a fine refinement box in the wake region to better capture the flow. Their dimensions are displayed in figure 6 with the characteristic lengths of the domain.

Table 1 Some of the domain sizes used in literature

Study	Lu	Ld	Lc	H
Zerihan (2001) [16]	10c	10c		7c
Mahon *et al.* (2005) [18]	1.32c	3.95c	3.10c	4.60c
Vogt *et al.* (2007) [24]	3c	9c	6c	5c
Doig *et al.* (2011) [25]	7c	15c		8c
Arrondeau *et al.* (2020) [14]	8c	15c	9c	10c
Angad (2023) [23]	9c	15c	8c	8c

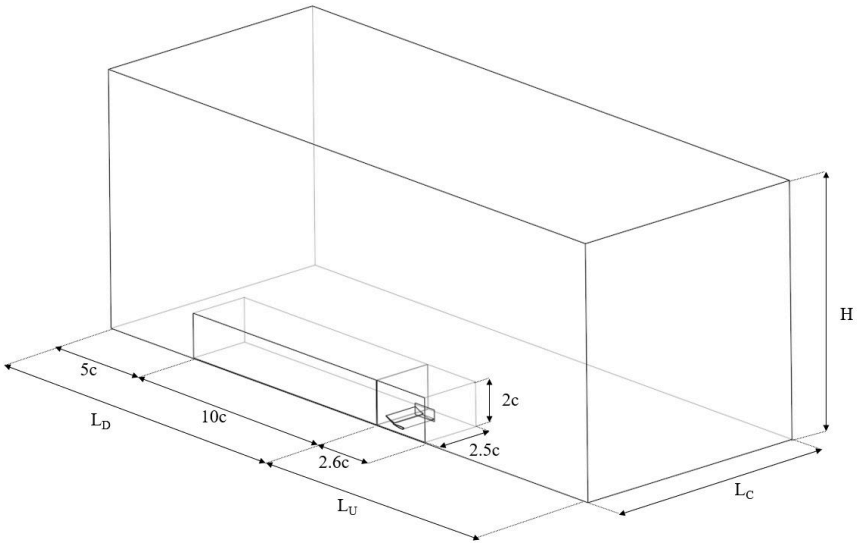

Fig. 6 Overview of the computational domain

D. Meshing strategy

The meshes were created using the Fluent 2023R2 meshing tool. All the generated meshes were hybrid: the farfield region consisted of polyhedral cells constituting the unstructured part and a structured mesh in the region close to the surfaces of geometries to better capture the boundary layers through the implementation of prism layers, as shown in figure 7 .

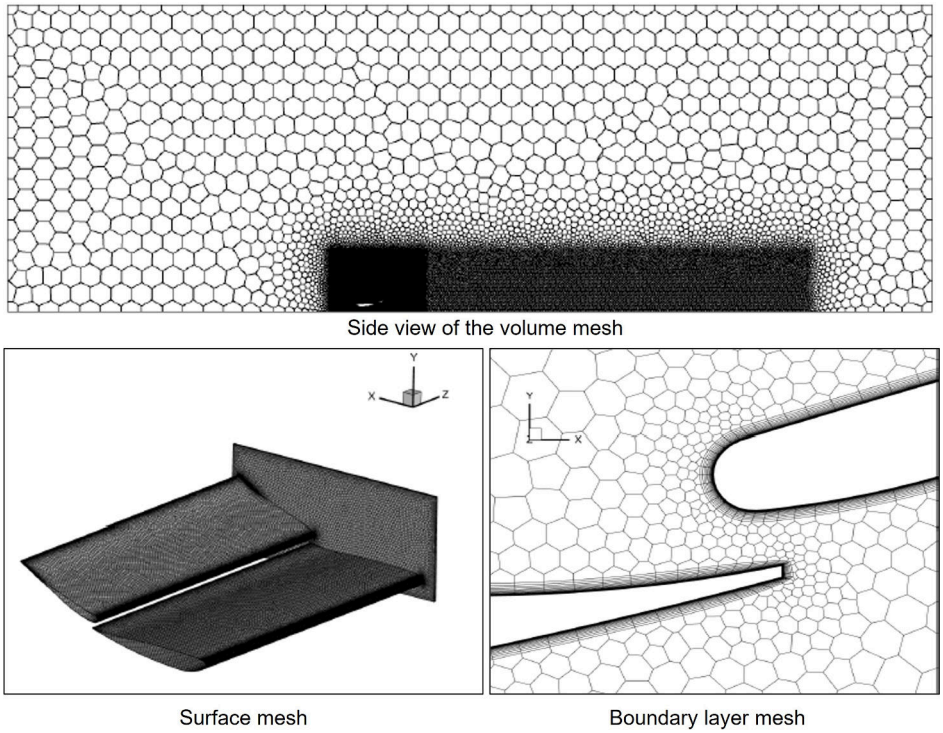

Fig. 7 Details of the Baseline Mesh

To better capture the viscous sub-layer, a y^+ of 1 was required on the surface of the geometry. For this, the initial spacing Δs at the walls had to be determined. Nonetheless, the dynamic viscosity μ needed to be known first using the formula for the Reynolds number (equation 1). The characteristic length of the wing was the normalised chord c = 380 mm. The freestream velocity was 30 m/s and the air density was assumed to be 1.225 kg/m^3.

$$Re = \frac{\rho U L}{\mu} \tag{1}$$

Wind tunnel experiments realised on this double-element front wing displayed a Reynolds number ranging from 0.735×10^6 to 0.765×10^6 [26]. This led to a range of the dynamic viscosity of $1.83 - 1.9 \times 10^{-5}$ kg/ms. Using an adequate y^+ calculator [27], gave the initial spacing Δs according to the desired value of the y^+. Furthermore, to determine the growth rate G_R and then generate the wanted number of prism layers, the boundary layer thickness δ had to be estimated. To do so, an analogy with the Blasius relation for turbulent flow flat plate was used [28, 29] (equation 2).

$$\delta \approx 0.038 \times \left(\frac{x}{Re_x^{1/5}} \right) \tag{2}$$

Therefore, $\delta = (9.61 - 9.69) \times 10^{-3}$. The boundary layer thickness δ was the sum of the n layers height related to the growth rate G_R by equation 3. The growth rate G_R could thus be calculated.

$$\delta = \sum_{k=0}^{n-1} {G_R}^k \Delta s \ = \Delta s \left(\frac{1 - G_R^n}{1 - G_R} \right) \tag{3}$$

For the boundary layer mesh, the last ratio method and the uniform method were compared. The last ratio method allowed the setting of the first cell height (Δs) and this value was maintained in all the regions where the boundary layer mesh was created. This method was effective for keeping the y^+ at the targeted value. However, this method does not allow for the setting of the growth rate. It was automatically adjusted to satisfy the transition ratio and the first height and thus, the boundary layer mesh thickness varies along the surface (see Figure 7). On the other hand, the uniform method allowed setting the first cell height, the number of prism layers, and the growth rate. It was effective

as it allows for more control of the meshing. Simulations on the baseline and tubercle configurations showed that the results were similar between the two methods. However, the last ratio method presented convergence issues (especially for large tubercle amplitude configurations). Thus, the uniform method was selected for the boundary layer mesh.

Two refinement boxes were created around the front wing geometry and in the wake region to better capture the flow physics and more accurately estimate the generated forces. A mesh grid convergence study was performed to select the parameters. Table 2 presents the sizing parameters to generate the meshes used in this study and figure 8 the grid convergence plot and the Richardson extrapolation.

Number of cells	4,200,000
y^+	1
Surface mesh sizing on wing surfaces	4
Surface mesh sizing at trailing edge	1
Main refinement region target cell size (mm)	8
Wake refinement region target cell size (mm)	16
Min. surface mesh size (mm)	0.5
Boundary layer first height (mm)	1.15×10^5
Number of layers	20
growth rate	1.2
Max. volume mesh size (mm)	200

Table 2 Meshing parameters

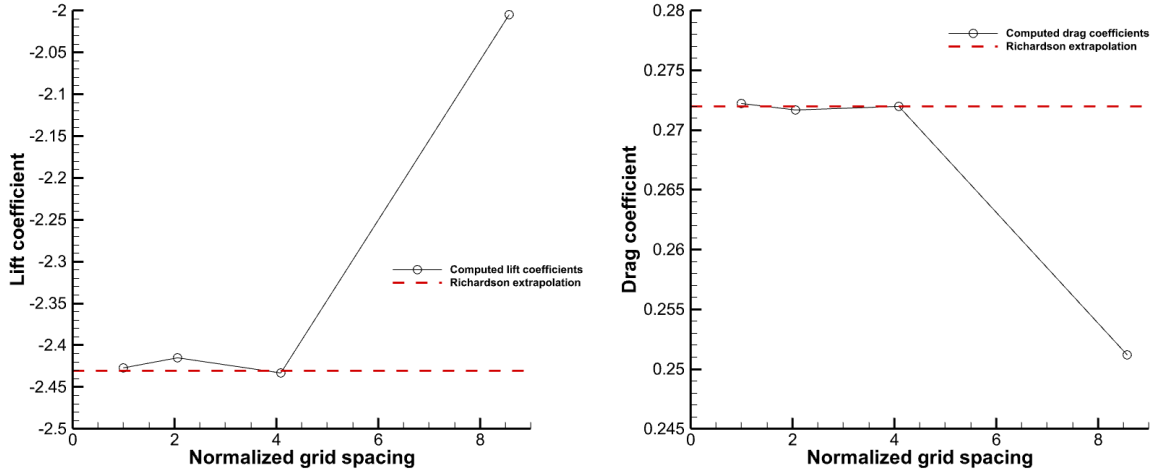

(a) Lift **(b) Drag**

Fig. 8 Grid convergence graph.

E. Numerical simulation setup

To perform the numerical simulations, the ANSYS Fluent 2023/R2 Computational Fluid Dynamics (CFD) software was used. The freestream velocity was set to 30m/s, which corresponds to a Mach number of $Ma = 0.087$. Therefore, the flow was assumed incompressible and a pressure-based solver was used to get steady-state solutions. Reynolds Average Navier Stokes (RANS) simulations were performed using the $\kappa - \omega$ Shear Stress Transport (SST) model. This

turbulence model was selected after comparing various models, as it offered the best accuracy for the validation case. The pressure-velocity coupling equation used scheme was the COUPLED scheme along with a Rie-Chow momentum-based flux type. Moreover, a first-order numerical discretization scheme simulation was performed until convergence for each configuration. Then, a second-order simulation was conducted based on the first-order simulation results. The air was assumed to be an ideal gas, with constant Specific heat and Thermal conductivity. The viscosity is modelled by Sutherland's law. To best reproduce the conditions of Zerihan's experiment, a velocity-inlet boundary condition was used with the freestream turbulence intensity set to 0.2% and the turbulent viscosity ratio to 10%. The temperature was set to 292.8K. The outlet was set as a pressure outlet with the same freestream conditions as the inlet. The ground was also set as a moving wall with no-slip condition to reproduce the moving belt used by Zerihan in his experiment. The ground moves at the same speed and direction as the airflow. The moving ground and the ground height definition are presented in figure 9. The top and side planes were modelled as symmetry boundary conditions to reproduce Zerihan's wind tunnel experiments.

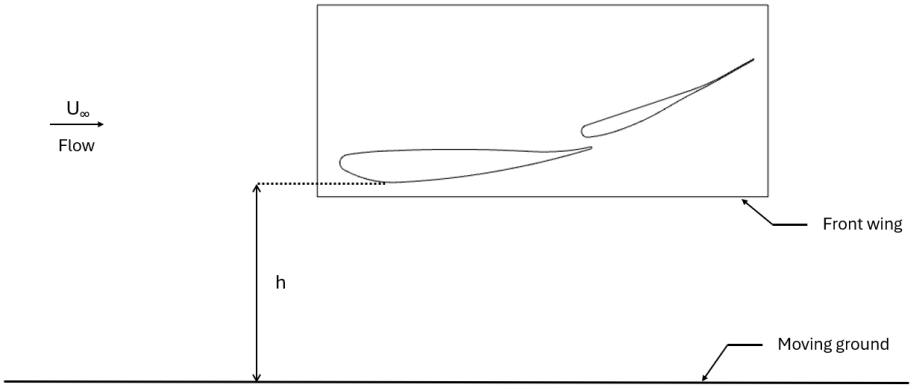

Fig. 9 Ground height definition.

IV. Results and discussion

A. Validation case

It was essential to validate the geometries, the meshes and the CFD setup to get accurate and qualitative results. To do so, the results of the simulations were compared with experimental data from Zerihan's study [16]. The CFD results were compared with the experimental results with the closest ground heights to each ride height tested.
Table 3 presents a comparison between the numerical and the experimental values. For both ride heights, the errors in lift and drag were lower than 10%. This informed that the results of the simulations were in line with the experimental values regarding the aerodynamic coefficients. Nonetheless, the lift was slightly under-predicted and the drag was overestimated. This resulted in a lift-to-drag ratio error higher than 10%. This could be linked to the limitations of the $\kappa - \omega SST$ model.

Table 3 CFD and experimental data comparison

	Experimental	CFD	Error (%)
C_L	-2.62	-2.43	7.14
C_D	0.25	0.27	8.80
L/D	-10.48	-8.95	14.65

(a) h/c=0.224

	Experimental	CFD	Error (%)
C_L	-2.88	-2.64	8.61
C_D	0.258	0.282	9.43
L/D	-11.8	-9.33	16.5

(b) h/c=0.134

The pressure plots from the simulations are compared with the experimental data collected by Zerihan [16] in figure 10. The errors between the numerical and the experimental value were around 10%, with a peak at 14% at x/c = 0.3, for

the case where h/c = 0.224 whereas they were slightly higher when h/c = 0.134, with a peak at 25% at the flap's leading edge. This value confirmed the previous observations: the pressure coefficients estimated by the simulations were in line with the experiments however lift slightly under-predicted and the drag was overestimated.

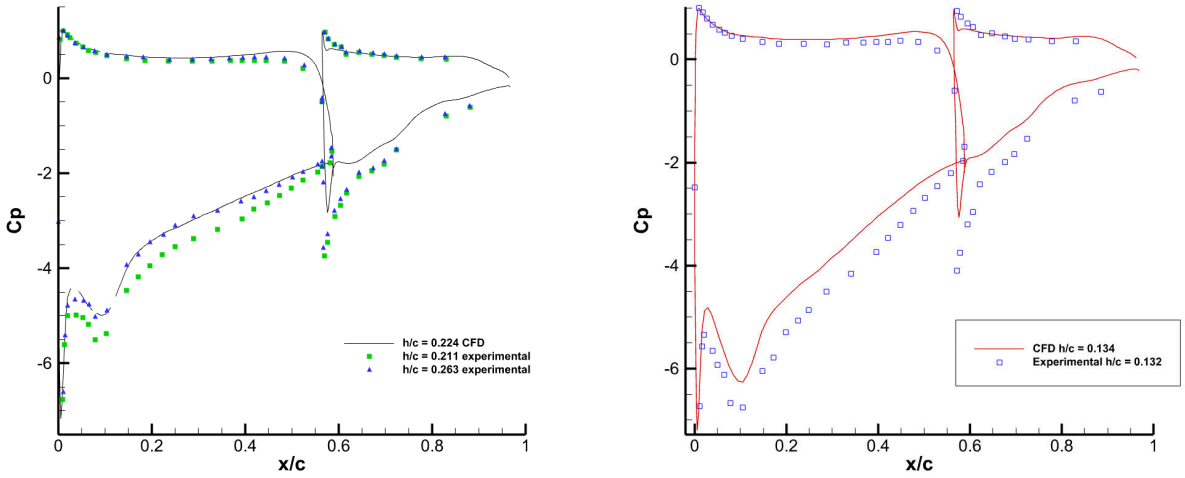

(a) h/c = 0.224 **(b) h/c = 0.134**

Fig. 10 Comparison of the chordwise pressure distributions for the baseline.

B. Impact of the tubercles

First, the effect of tubercle amplitude was studied. Since endplates were removed on tubercle configurations, they were also removed in the baseline configuration. Looking at Table 4, it was noticed that adding tubercles reduced the generated downforce for both ride heights for most configurations, especially those with large amplitude tubercles. The Cp plots in Figure 11 present reduced suction areas with pressure recovery starting at higher Cp values for models with large tubercles. By observing the X-velocity contours of large amplitude configurations in figure 13, separation bubbles at the troughs on the leading edges and flow separation under the flap were noticed, which could explain this reduction.

In addition, sets of counter-rotating vortices emanating from the leading edge of large amplitude tubercle troughs were observed on the Q-criterion figures (see Figure 14). The vortices at the flap troughs were stronger as they expand further downstream. In fact, the flow separation at the flap might induce these vortices. These vortices did not bring enough momentum to the boundary layer for reattachment. Moreover, the low-velocity magnitude suggested that these vortices did not generate downforce.

Nonetheless, at both ride heights, the addition of low-amplitude tubercles slightly increased the downforce. The Cp spike in figure 12 at the leading edges of troughs might explain this increase. In this case, the vortices contributed to increased mixing of the boundary layer, potentially helping to energise the flow near the surface and delay separation. However, this increase in downforce came at the expense of increased drag. It has increased for the configurations $MEF\_f_3\_2A004\_f_6\_2A002$ and $MEF\_f_3\_2A006\_f_6\_2A003$, while for the configurations with higher amplitude ($MEF\_f_3\_2A008\_f_6\_2A004$ and $MEF\_f_3\_2A010\_f_6\_2A005$) the drag significantly decreased at both ride heights. These variations in drag are due to the induced drag: separation consequently decreased lift which reduces lift-induced drag while for low amplitude configuration the increase in lift caused an increase in drag due to the lift induced drag. However, the lift-to-drag ratio reduced highlighting that the implementation of tubercles did not prove to be effective in that context.

Overall, the efficiency of the front wing with tubercles was reduced compared to the clean leading edge configuration. Efficiency decreased as the tubercle amplitude increased. Although only amplitudes below 10% of the chord were

studied, the observed trend suggested that higher amplitude tubercles would further deteriorate efficiency.

Table 4 Aerodynamic coefficients of the amplitude configurations

	Baseline (no endplate)	$MEF\_f_3\_2A004\_f_6\_2A002$	$MEF\_f_3\_2A006\_f_6\_2A003$	$MEF\_f_3\_2A008\_f_6\_2A004$	$MEF\_f_3\_2A010\_f_6\_2A005$
CL	-2.35	-2.36	-2.31	-1.83	-1.78
CD	0.28	0.29	0.28	0.25	0.25
L/D	-8.28	-8.25	-8.15	-7.32	-7.12

(a) $h/c = 0.224$

	Baseline (no endplate)	$MEF\_f_3\_2A004\_f_6\_2A002$	$MEF\_f_3\_2A006\_f_6\_2A003$	$MEF\_f_3\_2A008\_f_6\_2A004$	$MEF\_f_3\_2A010\_f_6\_2A005$
CL	-2.78	-2.79	-2.66	-1.97	-1.90
CD	0.31	0.31	0.31	0.27	0.27
L/D	-8.97	-8.92	-8.66	-7.23	-7.0

(b) $h/c = 0.134$

Moreover, the effects of the frequency were studied. Table 5 presents the aerodynamic coefficients of the configurations with different tubercle frequencies. Varying tubercle frequency did not make any major impact on the aerodynamics of the front wing, all the configurations at the same height present similar coefficients and flow characteristics. However, the ride height affects the results. At $h/c = 0.224$, the implementation of tubercles increased drag by 3.6% compared to the baseline model whereas the generated lift almost remains equal which caused the lift-to-drag ratio to decrease by -9%. On the other hand, at $h/c = 0.134$, downforce and drag remain almost identical. For both ride heights, the aerodynamic efficiency decreased of almost 1% at this ride height which is negligible. For all the configurations, reducing the ride height increases lift but drag slightly rises due to lift induced drag. However, lift-to-drag ratio is higher when the ride height decreases as studied by Zerihan [16].

Therefore, adding or reducing the number of tubercles did not have any meaningful impact on the flow. This did not align with Angad's results [23], as he observed an optimal tubercle frequency in his study. One possible explanation was that the tubercle amplitude in the frequency study might have been too low to significantly impact the results. Indeed, in the case of low-amplitude tubercles, no flow separation was observed, only the tip vortex was seen to generate more downforce compared to the baseline. The vortices generated at the troughs were minimal compared to those observed at higher amplitudes. Another explanation could be due to the fact that the tubercles were implemented by keeping a constant thickness-to-chord ratio which caused the front wing to be "wavy".

Table 5 Aerodynamic coefficients of the frequency configurations

	Baseline	$MEF\_f_3\_2A004\_f_6\_2A002$	$MEF\_f_4\_2A004\_f_8\_2A003$	$MEF\_f_5\_2A004\_f_{10}\_2A004$	$MEF\_f_6\_2A004\_f_{12}\_2A005$
CL	-2.45	-2.36	-2.36	-2.36	-2.36
CD	0.27	0.29	0.29	0.29	0.29
L/D	-9.02	-8.25	-8.25	-8.25	-8.25

(a) $h/c = 0.224$

	Baseline	$MEF\_f_3\_2A004\_f_6\_2A002$	$MEF\_f_4\_2A004\_f_8\_2A003$	$MEF\_f_5\_2A004\_f_{10}\_2A004$	$MEF\_f_6\_2A004\_f_{12}\_2A005$
CL	-2.64	-2.79	-2.78	-2.77	-2.77
CD	0.28	0.31	0.31	0.31	0.31
L/D	-9.34	-8.92	-8.91	-8.90	-8.90

(b) $h/c = 0.134$

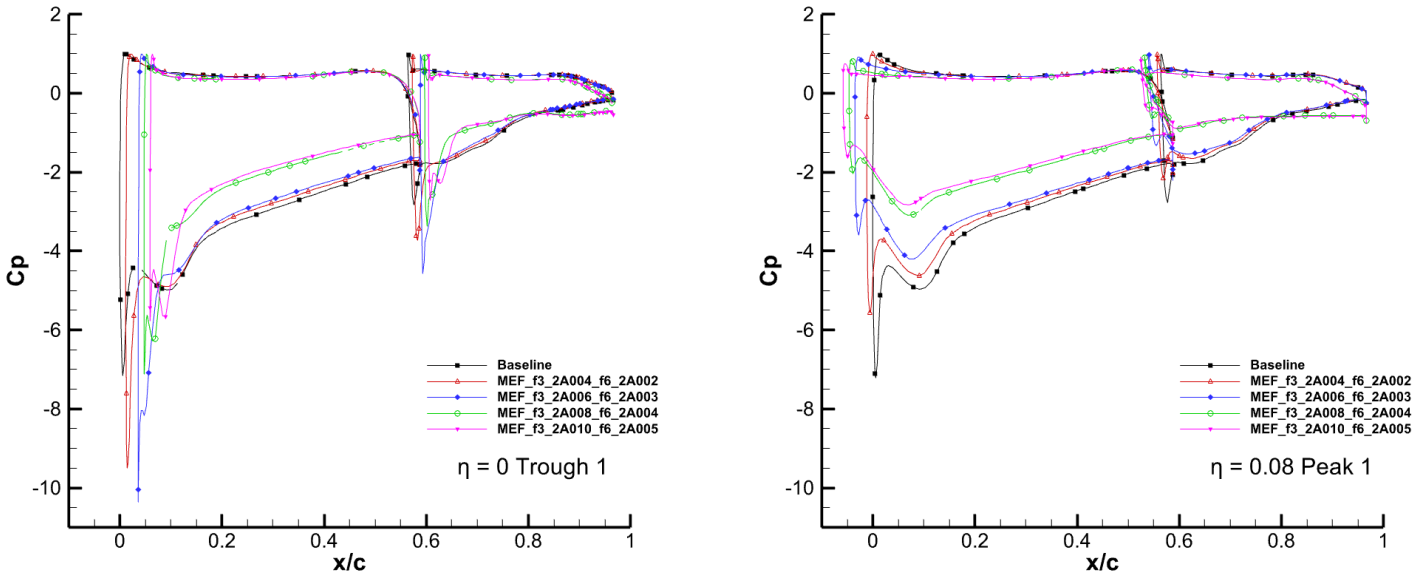

Fig. 11 Comparison of the pressure distributions of amplitude configurations at h/c=0.224

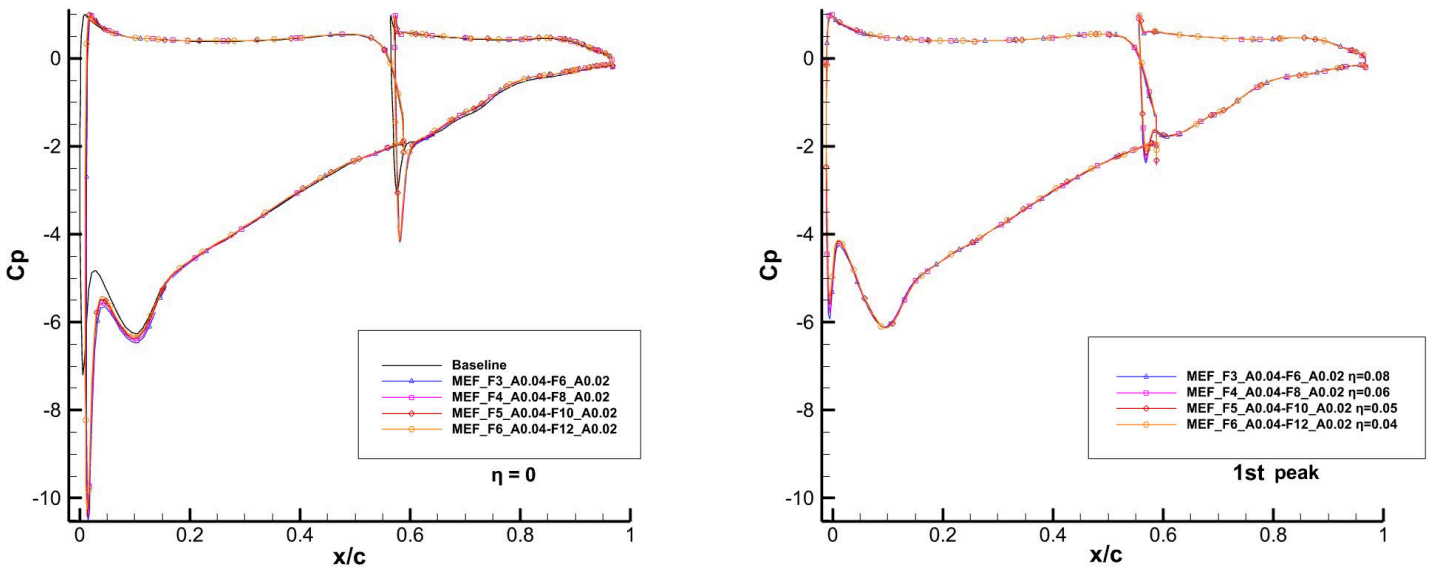

Fig. 12 Pressure distribution plots of the frequency configurations at h/c=0.134

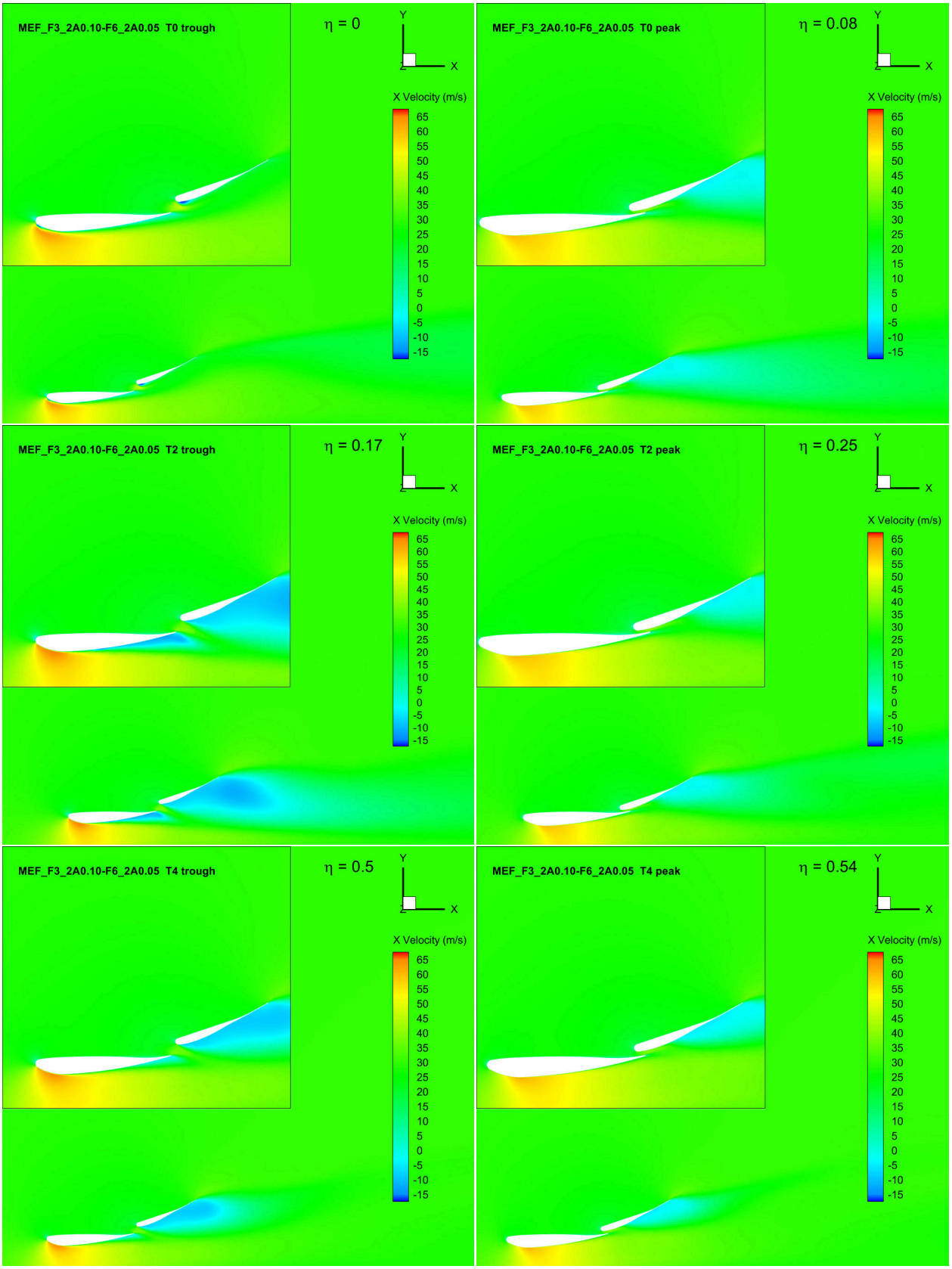

Fig. 13 X-velocity contours for MEF_F3_2A0.10-F6_2A0.05 model at h/c=0.134

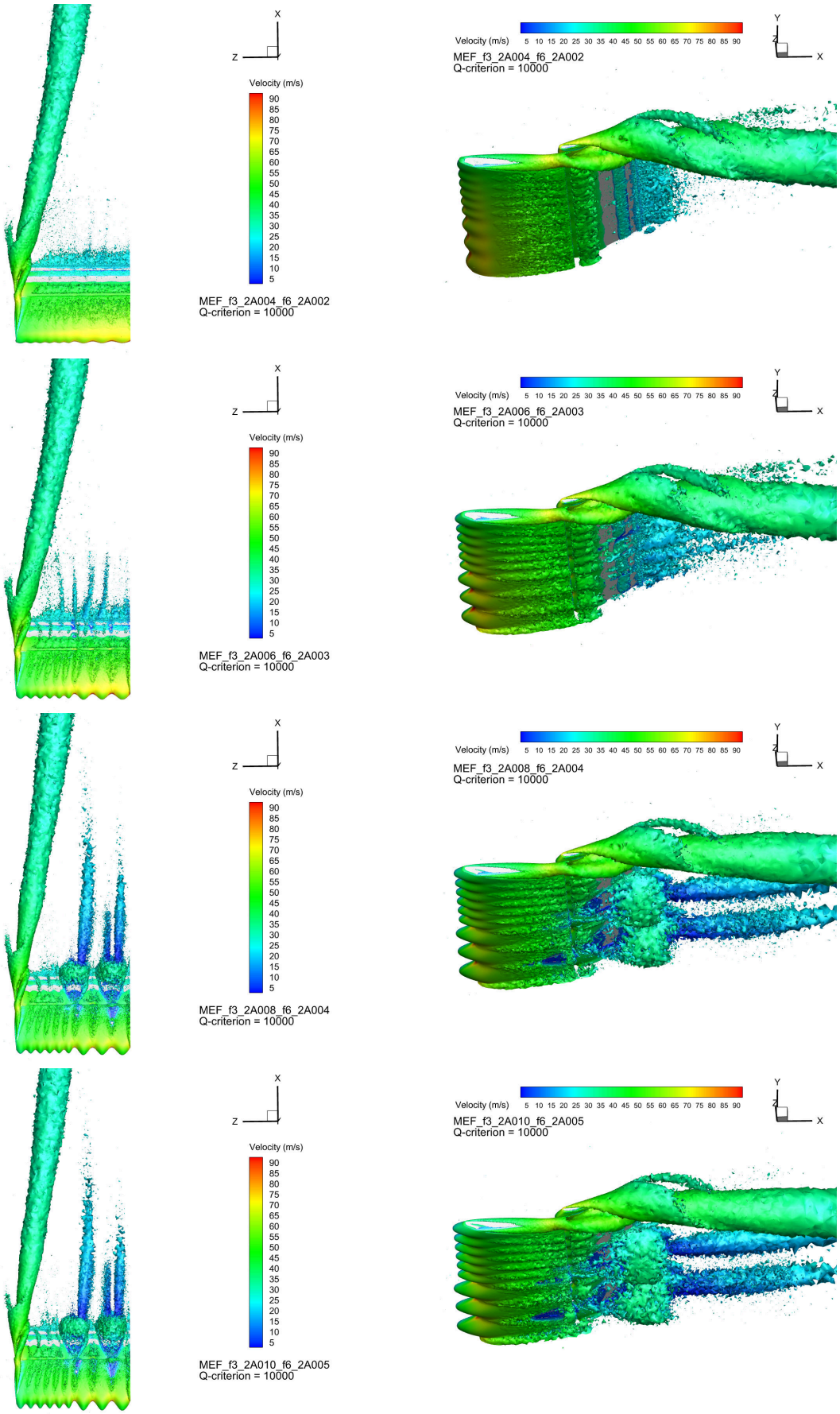

Fig. 14 Q-criterion iso-surface of the models with varying amplitude at h/c=0.224

V. Conclusion

This study investigated the aerodynamic effects of implementing bio-inspired tubercle distribution on F1 front wings in the presence of the ground effect. Two ground heights were studied ($h/c = 0.134$ and $h/c = 0.224$). Numerical simulations were conducted using $\kappa - \omega$ SST model. Various tubercle configurations with varying amplitudes and frequencies were tested. However, the results showed that bio-inspired tubercle distribution did not improve the front wing's aerodynamic efficiency. Models with higher amplitude tubercles significantly reduced downforce due to flow separation under the flap and at the troughs, further diminishing their aerodynamic efficiency.

Nonetheless, the study on tubercle amplitude resulted in interesting outcomes. The implementation of low-amplitude tubercles increased downforce compared to the clean leading-edge model for both ride heights. However, this came at the cost of increased drag due to induced lift. For both ride heights, the resulting Lift-to-Drag ratio was lower than that of the baseline model. Unlike previous studies [14, 23], where an optimal tubercle frequency was identified, this investigation into the frequency of tubercles showed that varying the number of tubercles along the wing had little to no impact on aerodynamic performance. This could be due to the low amplitude of the tubercles implemented, which were insufficient to cause significant flow disturbances. Another reason could be the thickness-to-chord ratio that is constant along the span, resulting in wavy front wings.

The results obtained suggest that tubercles may not function as effective vortex generators in the context of front wings in the ground effect, raising questions about their relevance in the context of F1. In fact, among the front wing tubercle configuration, the highest aerodynamic efficiency was achieved by the $MEF\_f_3\_2A004\_f_6\_2A002$, the model with the least tubercles and with the smallest amplitude. Previous studies demonstrated the effectiveness of tubercles in stall conditions. However, stall rarely occurred in the context of F1 front wings. Finally, it could be interesting to perform similar studies with varying flow conditions (velocity, yaw angle, angle of attack) to simulate stall conditions. Besides, the new 2026 F1 technical regulations can bring scenarios where tubercles can prove their effectiveness.

References

[1] Karbus, G., "Breach days," , ???? URL `https://georgekarbusphotography.com/portfolio/breach-days/`.

[2] Fish, F. E., and Battle, J. M., "Hydrodynamic design of the humpback whale flipper," *Journal of Morphology*, Vol. 225, 1995. https://doi.org/10.1002/jmor.1052250105.

[3] Watts, P., and Fish, F., "The influence of passive, leading edge tubercles on wing performance," *Proc. Twelfth Intl. Symp. Unmanned Untethered Submers. Technol., Durham New Hampshire*, 2001.

[4] Miklosovic, D. S., Murray, M. M., Howle, L. E., and Fish, F. E., "Leading-edge tubercles delay stall on humpback whale (Megaptera novaeangliae) flippers," *Physics of Fluids*, Vol. 16, 2004. https://doi.org/10.1063/1.1688341.

[5] Nierop, E. A. V., Alben, S., and Brenner, M. P., "How bumps on whale flippers delay stall: An aerodynamic model," *Physical Review Letters*, Vol. 100, 2008. https://doi.org/10.1103/PhysRevLett.100.054502.

[6] Pauley, W. R., and Eaton, J. K., "Experimental study of the development of longitudinal vortex pairs embedded in a turbulent boundary layer," *AIAA*, Vol. 26(7), 1987.

[7] Custodio, D., "The Effect of Humpback Whale-Like Leading Edge Protuberances on Hydrofoil Performance," *Ph.D. Thesis*, Vol. Ph.D., 2012.

[8] Pedro, H. T., and Kobayashi, M. H., "Numerical study of stall delay on humpback whale Flippers," 2008. https://doi.org/10.2514/6.2008-584.

[9] Bolzon, M. D., Kelso, R. M., and Arjomandi, M., "The effects of tubercles on swept wing performance at low angles of attack," 2014.

[10] Papadopoulos, C., Katsiadramis, V., and Yakinthos, K., "Influence of tubercles' spanwise distribution on swept wings for unmanned aerial vehicles," *Proceedings of the Institution of Mechanical Engineers, Part G: Journal of Aerospace Engineering*, Vol. 235, 2021. https://doi.org/10.1177/0954410020919583.

[11] Johari, H., Henoch, C., Custodio, D., and Levshin, A., "Effects of leading-edge protuberances on airfoil performance," *AIAA Journal*, Vol. 45, 2007, pp. 2634–2642. https://doi.org/10.2514/1.28497.

[12] Hansen, K. L., "Effect of leading edge tubercles on airfoil performance," *Ph.D. Thesis*, Vol. Ph.D., 2012.

[13] Hansen, K. L., Kelso, R. M., and Dally, B. B., "An investigation of three-dimensional effects on the performance of tubercles at low Reynolds numbers," 2010.

[14] Arrondeau, B., and Rana, Z. A., "Computational aerodynamics analysis of non-symmetric multi-element wing in ground effect with humpback whale flipper tubercles," *Fluids*, Vol. 5, 2020. https://doi.org/10.3390/fluids5040247.

[15] Srinivas, K. S., Datta, A., Bhattacharyya, A., and Kumar, S., "Free-stream characteristics of bio-inspired marine rudders with different leading-edge configurations," *Ocean Engineering*, Vol. 170, 2018. https://doi.org/10.1016/j.oceaneng.2018.10.010.

[16] Zerihan, J. D. C., "An Investigation into the Aerodynamics of Wings in Ground Effect," , 2001.

[17] Zhang, X., Toet, W., and Zerihan, J., "Ground effect aerodynamics of race cars," , 2006. https://doi.org/10.1115/1.2110263.

[18] Mahon, S. A., "The Aerodynamics of Multi-Element Wings in Ground Effect," *Ph.D. Thesis*, Vol. Ph.D., 2005.

[19] Genua, E., "A CFD Investigation into Ground Effect Aerodynamics," *Msc. Thesis*, Vol. Msc., 2009.

[20] Bang, C. S., Rana, Z. A., Könözsy, L., Rodriguez, V. M., and Temple, C., "Aeroelastic Analysis of a Single Element Composite Wing in Ground Effect Using Fluid–Structure Interaction," *Journal of Fluids Engineering*, Vol. 144, No. 4, 2022, p. 041202. https://doi.org/10.1115/1.4053089, URL https://doi.org/10.1115/1.4053089.

[21] Bang, C. S., Rana, Z. A., Könözsy, L., Marchante Rodriguez, V., and Temple, C., "Numerical Investigation and Fluid-Structure Interaction (FSI) Analysis on a Double-Element Simplified Formula One (F1) Composite Wing in the Presence of Ground Effect," *Fluids*, Vol. 7, No. 2, 2022. https://doi.org/10.3390/fluids7020085, URL https://www.mdpi.com/2311-5521/7/2/85.

[22] Castro, X., and Rana, Z. A., "Aerodynamic and Structural Design of a 2022 Formula One Front Wing Assembly," *Fluids*, Vol. 5, No. 4, 2020. https://doi.org/10.3390/fluids5040237, URL https://www.mdpi.com/2311-5521/5/4/237.

[23] Singh, A., "Adjoint Optimisation And Computational Aerodynamic Analysis Of A Bio-Inspired Double Element Front Wing," *MsC. Thesis*, Vol. MsC, 2023.

[24] Vogt, J. W., Barber, T. J., and Leonardi, E., "Flow field phenomena about lift and downforce generating cambered aerofoils in ground effect," 2007.

[25] Doig, G., Barber, T. J., and Neely, A. J., "The influence of compressibility on the aerodynamics of an inverted wing in ground effect," *Journal of Fluids Engineering, Transactions of the ASME*, Vol. 133, 2011. https://doi.org/10.1115/1.4004084.

[26] Zhang, X., and Zerihan, J., "Aerodynamics of a Double-Element Wing in Ground Effect," *AIAA Journal*, Vol. 41, No. 6, 2003, pp. 1007–1016. https://doi.org/10.2514/2.2057, URL https://doi.org/10.2514/2.2057.

[27] "CFD Online, Y+ Wall Distance Estimation," , ???? URL https://www.cfd-online.com/Tools/yplus.php.

[28] Schlichting, H., and Gersten, K., *Boundary-Layer Theory*, 2016. https://doi.org/10.1007/978-3-662-52919-5.

[29] Sakiadis, B. C., "Boundary-layer behavior on continuous solid surfaces: I. Boundary-layer equations for two-dimensional and axisymmetric flow," *AIChE Journal*, Vol. 7, 1961. https://doi.org/10.1002/aic.690070108.

Impact of whale tubercles on the aerodynamics characteristics of F1 front wing - adjoint optimization

Toprakoglu, Fidel

2025-01-06

Toprakoglu F, Ozyumruoglu I, Rana ZA, Di Pasquale D. (2025) Impact of whale tubercles on the aerodynamics characteristics of F1 front wing - adjoint optimization. AIAA SCITECH 2025 Forum, 6-10 January 2025 Orlando, FL. Paper number AIAA 2025-0479

https://doi.org/10.2514/6.2025-0479